A Comparative Study of Turbulence Models Performance for Turbulent Flow in a Planar Asymmetric Diffuser

Samy M. El-Behery, and Mofreh H. Hamed

Abstract—This paper presents a computational study of the separated flow in a planer asymmetric diffuser. The steady RANS equations for turbulent incompressible fluid flow and six turbulence closures are used in the present study. The commercial software code, FLUENT 6.3.26, was used for solving the set of governing equations using various turbulence models. Five of the used turbulence models are available directly in the code while the v2-f turbulence model was implemented via User Defined Scalars (UDS) and User Defined Functions (UDF). A series of computational analysis is performed to assess the performance of turbulence models at different grid density. The results show that the standard k-ω, SST k-ω and v2-f models clearly performed better than other models when an adverse pressure gradient was present. The RSM model shows an acceptable agreement with the velocity and turbulent kinetic energy profiles but it failed to predict the location of separation and attachment points. The standard k-ε and the low-Re k-ε delivered very poor results.

Keywords—Turbulence models, turbulent flow, wall functions, separation, reattachment, diffuser.

I. INTRODUCTION

THE equations governing single-phase flows, the so-called Navier-Stokes equations have been known for more than a century. Despite intensive researches have been made; direct analytical solutions to these equations are not available, except for a very limited number of special cases. Since digital computers became available in the 1960's, the analysis of single-phase flows have increasingly been carried out numerically using a range of techniques which together form the field known as Computational Fluid Dynamics, CFD, [1]. In the present time, Computational Fluid Dynamics tools are becoming standard in many fields of engineering involving flow of gases and liquids; numerical simulations are used both in the design phase to select between different concepts and in the production phase to analyze performance.

Turbulence has a decisive influence on heat transfer, species transport, drag, vorticity distribution, separation and swirl flow. Separation and reattachment of turbulent shear layers in the presence of adverse pressure gradient can be seen in many practical industrial and engineering applications, either in internal flow systems such as diffusers, combustors and channels with sudden expansion, or in external flows like those past bluff structures and buildings. Turbulent flows are characterized by fluctuating velocity fields. Therefore, one way is to use a numerical mesh finer than the smallest length scales and time step smaller than the fastest fluctuations of the flow. This method is usually called Direct Numerical Simulations (DNS). The exact governing equations can be time-averaged, ensemble-averaged, or manipulated to remove the small scales, resulting in equations that are computationally less extensive to solve. However, the modified equations contain additional unknown variables, and thus the turbulence models are needed to determine these variables in terms of known quantities. Generally, both the Reynolds–averaged Navier-Stokes approach (RANS) and the Large Eddy Simulation (LES) approach can be employed to transform the Navier-Stokes equations in such a way that the small scale turbulent fluctuations do not have to be directly simulated. However, here, only the Reynolds–averaged approach is considered for the simulation of flow through asymmetric diffuser based on the following three factors: (1) the mean flow in the diffuser is steady, (2) large computer resources are required to resolve the energy–containing turbulent eddies if LES approach is used, (3) the Reynolds-averaged approach has been proven to be suitable for industrial fluid simulations [1 and 2]. The RANS equations need a turbulence model for computation of Reynolds stresses that stems from averaging the non-linear convective terms, see for more details [3]. A large family of turbulence models exists in the literature which is far too extensive to be reviewed here. The models are ranged from simple algebraic expressions for the eddy viscosity to more elaborate formulations which introduce a separate transport equation for each component of the Reynolds stresses, see for more details [4 and 5].

The most popular turbulence models are the standard k-ε model [6], low-Re k-ε model [7], RNG k-ε model [8], standard k-ω model [9], SST k-ω model [10]. These are based on Boussinesq assumption that relates the apparent turbulent shearing stresses to the rate of mean strain through an apparent scalar turbulent or "eddy" viscosity. Consequently, the relation between the Reynolds stresses and the velocity

Samy M. El-Behery is with Faculty of Engineering, Menoufiya University, Shebin El-kom, Egypt (e-mail: s_elbehery@yahoo.com).
Mofreh H. Hamed is with Faculty of Engineering, Kafrelsheikh University, Kafrelsheikh, Egypt (e-mail: mofrehhh@yahoo.com).

World Academy of Science, Engineering and Technology
International Journal of Aerospace and Mechanical Engineering
Vol:3, No:5, 2009

gradient is linear. The v2-f turbulence model is a recently developed four equation turbulence model [11]. This model is similar to the standard k-ε model, and incorporates also some near-wall turbulence anisotropy as well as non-local pressure-strain effects. A more general model than those based on the Boussinesq assumption is the Reynolds stress model [12]. In this model, a separate transport equation for each component of the Reynolds stresses is solved. Turbulence modeling is commonly faulted as the case of deviations from measured data in the predictions of flow through the tested case. Therefore, turbulence modeling is a key issue in most CFD simulations. Virtually all engineering applications are turbulent and hence required turbulence model. Nevertheless, no pretence has been made that any of these models can be applied to all turbulent flows: such as 'universal' model may not exist. Each Model has its advantages, disadvantages, limitations and appropriate flow regimes. Industry has many pressing flow problems to solve that will not wait for the conception of a universal turbulence model. Fortunately, many sectors of industry are specifically interested in a limited class of flows only; e.g. pipe flows for the oil transportation sectors and diffusers for jet engines and compressors. The large majority of turbulence research consists of case-by-case examination and validation of existing turbulence models for such specific problems. Performance of a propulsion system as a whole is dependent on the efficiency of diffusers. Therefore, identification of separation within diffusers is important because separation increases drag and causes inflow distortion to engine fans and compressors. Diffuser flow computations are a particularly challenging task for Computation Fluid Dynamics (CFD) simulations due to adverse pressure gradients created by the decelerating flow, frequently resulting in separation. These separations are highly dependent on local turbulence level, viscous wall effects, and diffuser pressure ratio, which are functions of the velocity gradients and the physical geometry. Thus, turbulence modeling and geometry modeling become dominant factors that affect the ability of CFD to accurately predict flow through diffusers.

Therefore, the goal of this study is to examine six turbulence models in terms of their accuracy, convergence and computational cost. In addition, comparisons are made between FLUENT code and WIND code predictions for some of these turbulence models.

II. MATHEMATICAL MODEL AND COMPUTATIONAL METHOD

The commercial FLUENT software package, FLUENT 6.3.26, was used for solving the set of governing equations. The numerical method employed is based on the finite volume approach. Fluent provides flexibility in choosing discretization schemes for each governing equation. The discretized equations, along with the initial condition and boundary conditions, were solved using the segregated solution method. Using the segregated solver, the conservation of mass and momentum were solved sequentially

and a pressure-correction equation was used to ensure the conservation of momentum and the conservation of mass (continuity equation). Several turbulence models, such as, the standard k–ε model, the low-Re k–ε model, the standard k–ω model, the shear-stress transport k–ω model, the Reynolds stress model (RSM) and the v2-f model. The first five models are available directly in FLUENT while the last one (v2-f model) was implemented using user defined functions (UDF) and user defined scalars (UDS).

A. Governing Equations

In the present study steady RANS equations for turbulent incompressible fluid flow with constant properties are used. The governing flow field equations are the continuity and the Reynolds averaged Navier-Stokes equations, which are given by:

$$\frac{\partial u_i}{\partial x_j} = 0.0 \tag{1}$$

$$\frac{\partial u_i u_j}{\partial x_j} = -\frac{1}{\rho}\frac{\partial p}{\partial x_i} + \frac{\partial}{\partial x_j}\left(\nu S_{ij} \quad \overline{u_i' u_j'}\right) \tag{2}$$

Where, S_{ij} is the main strain rate and calculated by:

$$S_{ij} = \frac{1}{2}\left(\frac{\partial u_i}{\partial x_j} + \frac{\partial u_j}{\partial x_i}\right) \tag{3}$$

and $\overline{u_i' u_j'} = \tau_{ij}$ is the unknown turbulent or Reynolds-stress tensor and u_i' represents the velocity fluctuation in i-direction. These equations are not a closed set and turbulence models are required to model the turbulent or Reynolds-stress tensor.

B. Turbulence Modeling

Several turbulence models available are employed to predict the flow behavior in a planer asymmetric diffuser. Most of these models are derived from standard k–ε model and vary in complexity and robustness from two equation turbulence models to more elaborated turbulence model. Five of the used turbulence models are based on the Boussinesq assumption. In which the Reynolds stress tensor is computed from the effective viscosity formulation, which is a direct extension of the laminar deformation law. It is given by:

$$\tau_{ij} = \frac{2}{3}k\,\delta_{ij} - 2\,\nu_t S_{ij} \tag{4}$$

Where, $k = \overline{u_i' u_j'}$ is the turbulent kinetic energy, δ_{ij} is the Kronecker delta and ν_t denotes turbulent kinematic viscosity. In order to obtain the turbulent viscosity, other transport equations are needed. Theses equations differ from model to another.

1. The Standard k–ε model (SKE)

The k–ε model is well described in the literature and has been widely used. This model was derived by assuming that the flow is fully turbulent and the effects of molecular viscosity are negligible [6]. For locations near walls, the

World Academy of Science, Engineering and Technology
International Journal of Aerospace and Mechanical Engineering
Vol:3, No:5, 2009

standard k-ε model, therefore, demands an additional model, which comprises the effects of molecular viscosity. In this situation, wall functions based on semi-empirical formulas and functions are employed.

2. Low Reynolds Number k–ε Model (LRNKE)

The Low-Reynolds-number k–ε model of Launder and Sharma [7] is similar to the standard k–ε model except that is uses damping function instead of the wall-function and contains extra source terms in its turbulent kinetic energy and dissipation rate equations. Patel et al. [13] reviewed several low-Re k-ε model and they found that the model of Launder and Sharma performs better than the others. Furthermore, the model of Launder and Sharma uses the turbulent Reynolds number in the damping function instead of the dimensionless wall distance, Y^+. This makes the model suitable for simulating flow when separation is expected. While, the models which use Y^+ are not the right choice for separated flow problems (since Y^+ vanishes at separation and reattachment locations driving f_μ to zero, creating laminar spots in the middle of a turbulent flow). The turbulent kinetic energy, k, equation for the standard and the low-Re k-ε models reads

$$\frac{\partial}{\partial x_j}(\rho u_j k) = \frac{\partial}{\partial x_j}\left\{\frac{\mu_{eff}}{\sigma_k}\frac{\partial k}{\partial x_j}\right\} + G - \rho D \quad (5)$$

Where, the turbulent production rate is

$$G = \mu_{eff}\left(\frac{\partial u_i}{\partial x_j} + \frac{\partial u_j}{\partial x_i}\right)\frac{\partial u_i}{\partial x_j} \quad (6)$$

The dissipation rate, ε, equation for the standard and the low-Re k-ε models reads

$$\frac{\partial}{\partial x_j}(\rho u_j \varepsilon) = \frac{\partial}{\partial x_j}\left\{\frac{\mu_{eff}}{\sigma_\varepsilon}\frac{\partial \varepsilon}{\partial x_j}\right\}$$
$$+ (C_{\varepsilon 1}f_1 G - C_{\varepsilon 2}f_2 \rho \varepsilon)\frac{\varepsilon}{k} + E \quad (7)$$

The models constants $C_{\varepsilon 1}$ and $C_{\varepsilon 2}$, the damping functions f_1, f_2 and f_μ, and the extra source terms D and E for the low-Re k–ε model can be found in [6, 7].

3. The Standard k- ω model (SKW)

The standard k-ω model is one of the most common turbulence models. It includes two extra transport equations to represent the turbulent properties of the flow. The first transported variable is turbulent kinetic energy, k, similar to the turbulent kinetic energy equation of the standard k-ε model. The second is the specific dissipation, ω, which can also be thought of as the ratio of ε to k [9]. The model incorporates modifications for low-Re effects, compressibility and shear flow spreading. Detailed derivations for the closure equations are provided by Wilcox [9].

4. The Shear Stress Transport k- ω (SST)

The SST k- ω model was developed by Menter [10], which combined the robustness of k-ω turbulence model near walls with capabilities of the k-ε model away from the walls. The

definition of the turbulent viscosity is modified to account for the transport of turbulent shear stress. The model equations are provided in [10].

5. The Reynolds Stress Model (RSM)

The Reynolds stress model (RSM) is a higher level, elaborate turbulence model. It is usually called a Second Order Closure. This modeling approach originates from [12]. In RSM, the eddy viscosity approach has been discarded and the Reynolds stresses are directly computed. The exact Reynolds stress transport equation accounts for the directional effects of the Reynolds stress fields. Detailed derivations for the closure equations are provided in [14].

6. v^2-f Turbulence Model (V2F)

This model is a simplification of the elliptic relaxation Reynolds stress model developed by Durbin [11], which requires the solution of three transport and one elliptic (relaxation) equations. The system of Reynolds stress equations is replaced by a transport equation for a velocity scalar ($\overline{v'^2}$) and an elliptic equation for (f). The model was reformulated to avoid the numerical oscillations of wall boundary for f, as given in [15]. The equations for turbulent kinetic energy and the dissipation rate are the same as those of the standard k-ε model, while the equations for $\overline{v'^2}$ and f can be written as given in [15] as follows

$$u_j \frac{\partial \overline{v'^2}}{\partial x_j} = kf - 6\overline{v'^2}\frac{\varepsilon}{k} + \frac{\partial}{\partial x_j}\left[(v + v_t)\frac{\partial \overline{v'^2}}{\partial x_j}\right] \quad (8)$$

$$L^2 \frac{\partial^2 f}{\partial x_j^2} - f = \frac{1}{T}\left[(C_1 - 6)\frac{\overline{v'^2}}{k} - \frac{2}{3}(C_1 - 1)\right] - C_2\frac{G}{k} \quad (9)$$

$$T = \max\left[\frac{k}{\varepsilon}, 6\sqrt{\frac{v}{\varepsilon}}\right] \quad (10)$$

$$L = C_L \max\left[\frac{k^{3/2}}{\varepsilon}, C_\eta\left(\frac{v^3}{\varepsilon}\right)^{1/4}\right] \quad (11)$$

The model constants are taken as given in [15]

C. Wall Functions

In the region near the wall, the gradient of quantities is considerably high and requires fine grids close to the wall to capture the changes of quantities. For complex flows where separation flow and reattachment occur, the conventional logarithmic wall-function proposed by Launder and Spalding [6] becomes less reliable. The non-equilibrium wall-function proposed by Kim and Choudhury is proven to give better predictions due to the fact that it accounts for the effects of pressure gradient and departure from equilibrium [17]. The standard k-ε model and the RSM model employ the non-equilibrium wall-function is applied to the wall-adjacent cells, while the low-Re k-ε model uses damping functions instead of the wall-function. The v^2-f model treats the near-wall turbulence without the use of exponential damping or wall functions. For the standard and SST k-ω models, if the

World Academy of Science, Engineering and Technology
International Journal of Aerospace and Mechanical Engineering
Vol:3, No:5, 2009

transitional flows option is enabled in the viscous model panel, low-Reynolds-number variants will be used, and, in that case the near-wall grids have to be very fine to obtain better predictions for the near wall modeling. If transitional flows option is not active as in the present study, the near wall grids follow a rule of the wall function [14].

The use of a wall function in a computational flow solver allows fewer points to be placed near the walls where as points are typically placed to $Y^+ = 1$ for a wall integrated grid. In the present study three wall functions with initial grid point spacing ranges from $Y^+ = 1$ to 30 are used near the wall in a wall function grid. These values of Y^+ were chosen to asses FLUENT's wall function capabilities across several positions in the boundary layer logarithmic region. The effect of the initial grid point spacing is investigated in this paper.

D. Diffuser Geometry and Computational Grids

The test case analyzed in this study is a two-dimensional turbulent flow in an asymmetric planar diffuser. Due to the adverse pressure gradient the flow is separated and a large recirculation bubble is generated. This problem has been selected because a very reliable experimental database is available [17 and 18]. Moreover, a detailed Large Eddy Simulation study is also available for comparison [19].

The diffuser geometry is presented in Fig. 1 and the computational domain is shown in Fig.2. The tested diffuser can be divided into three sections: an inflow channel, the asymmetric diffuser, and an outflow channel. The upstream channel was made sufficiently long to obtain fully developed turbulent channel flow at the inlet of the diffuser section. The Reynolds number based on the bulk velocity and the upstream channel height, H, is 18000 matches the experimental configuration of Obi et al. [17] and Buice & Eaton [18].

In order to assess the grid sensitivity of the present results, Simulations were performed on three different meshes. The mesh is stretched in the streamwise and wall-normal directions and designed such that the streamwise spacing gradually decreases towards the diffuser. The refined grid was obtained by approximately doubling the number of points in y-direction. A detailed view of the coarse and fine grids at the diffuser inlet section is shown in Fig. 3.

E. Boundary Conditions

There are three faces bounding the calculation domain namely: the inlet boundary, the wall boundary and the outlet boundary. No-slip boundary conditions are applied along the solid walls and wall functions were used as described earlier. At the outlet, 60H downstream the diffuser exit, the boundary was adjusted as a pressure outlet boundary condition. At the inlet, 74H upstream the diffuser entrance, flat velocity and turbulent quantities profiles are specified.

F. Solution Strategy and Convergence

A second-order upwind discretization scheme was used for the momentum equation while a first-order upwind discretization was used for turbulent quantities. These schemes ensured, in general, satisfactory accuracy, stability and convergence. SIMPLE algorithm described by Patankar [20] was used for pressure-velocity coupling. The discretized equations are solved implicitly in sequence, starting with the pressure equation followed by the momentum equations, by the pressure correction equation, and finally by the equations for the scalars (turbulence variables). Within this loop, the linearized equations for each variable are integrated using a linear system solver. FLUENT code allows implementing customized models through user defined functions, UDF, which is treated for v^2-f turbulence model. Four user defined scalars, UDS, are used for this purpose. The wall-boundary condition of the dissipation rate equation depends on the turbulent kinetic energy, k, near the wall; therefore, it is necessary to initialize the solution before hooking the boundary condition.

The convergence criterion consisted of monitoring skin friction values and variation of velocity profiles with iteration, reduction of several orders of magnitude in the residual errors.
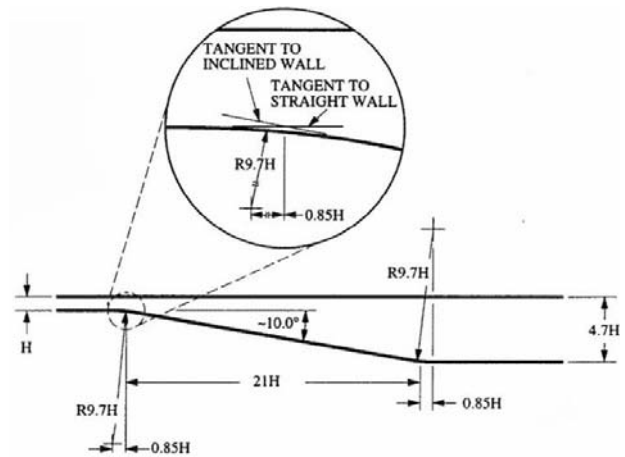

Fig. 1 Schematic of Buice-Eaton diffuser, Ref. [18]

III. RESULTS AND DISCUSSION

Steady flow in a planer asymmetric diffuser shown in Fig. 1 is investigated. Separated flow simulations in the tested diffuser were carried out using several turbulence models and three different meshes. The measured skin friction coefficient, C_f, in the fully developed entrance region is 0.0061. This value of C_f is used to calculate the initial wall spacing, y_p, as follows:

$$Y^+ = \frac{y_p u_\tau}{\nu}$$

Where, $\quad u_\tau = \sqrt{\tau_w / \rho} \quad ; \quad \tau_w = \frac{1}{2} C_f \ U_b^2 \quad \rho$

The variation of the dimensionless wall distance, Y^+, for the lower wall adjacent cell is presented in Fig. 4. It can be seen from this figure that Y^+ drops in the tail duct to approximately one-third its value in the upstream entrance region. In addition,
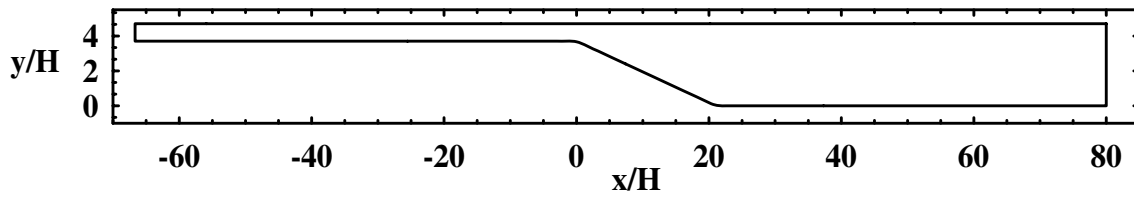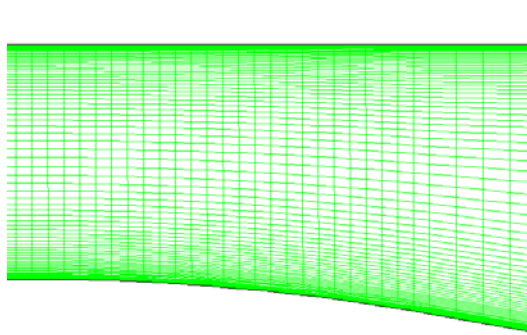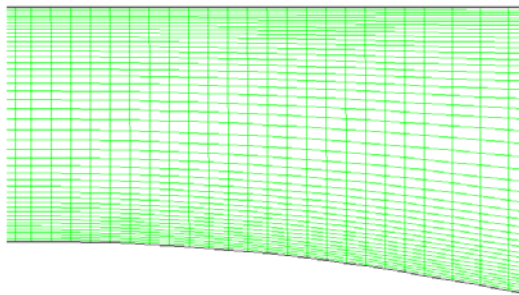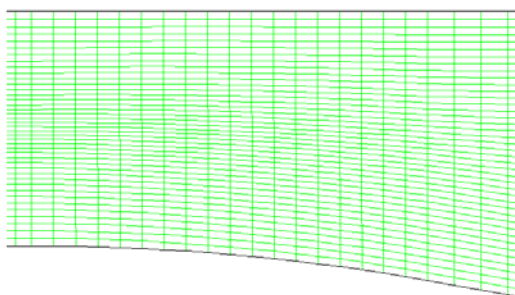
Fig. 2 Computational domain

a- fine grid ($Y^+ \approx 1.0$) 421×79

b- coarse grid ($Y^+ \approx 15$) 421×41
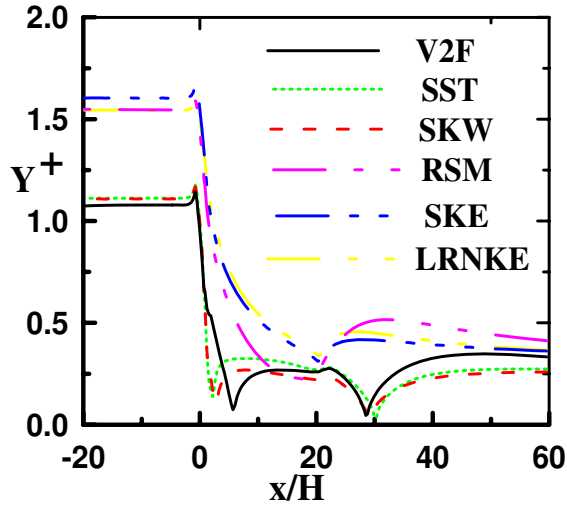

c- coarse grid ($Y^+ \approx 30$) 421×41

Fig. 3 Computational grid at diffuser inlet section

it was difficult to obtain a converged solution using LRNKE with the coarse girds. Therefore, the results presented here study for LRNKE was obtained with fine grid only (i.e., $Y^+= 1$).
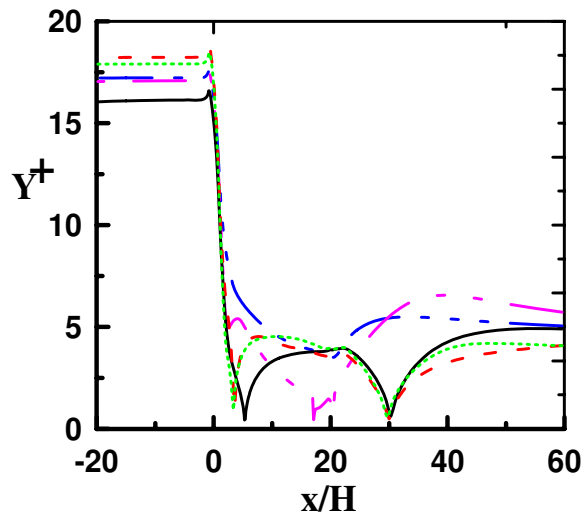
Figs. 5-6 show Comparisons between present predictions of pressure recovery coefficient using all the tested turbulence models and the experimental data of [17 and 18], and LES, results of [19]. It can be seen from the figures that most of the pressure increase occurs within the first third of the diffuser with the steepest rise at about $x/H = 1.5$. The figures also indicate that, in the case of fine grid, the pressure recovery coefficient obtained with V2F and SSTKW models agree reasonably well with experimental data of [17] and LES results of [19], while, LES predictions are higher than experimental data of [18] by about 5%. Also the SKE and LRNKE models predictions are closed to each other and are higher than the experimental data of [17 and 18] and LES results by about 20% in the separation region. The RSM predictions are close to experimental data of [18] rather than that of [17] and LES results, while the SKW model slightly over-predicts the pressure recovery coefficient when the fine grid is used. In the case of coarse grid all models predictions expect the SKE model are close to each other. The later still over-predict the pressure recovery coefficient, as shown in Fig. 6.

For incompressible, inviscid flow the total pressure recovery coefficient, $C_{po} = C_p + (U/U_b)^2$, is constant along a stream tube. A similar relation holds for viscous flow, declaring that the total pressure decreases in the flow direction due to frictional losses [19]. Fig. 7 shows comparisons between predicted total pressure recovery coefficient and normalized maximum velocity, U_{max}/U_b, and published experimental data and LES results of [19]. It can be seen from the figure that the SKE and LRNKE models under-predicts the maximum velocity in the rear part of the diffuser and in the downstream duct, while the RSM over-predicts the maximum velocity up to $x/H = 13$ and slightly under-predicts it after $x/H = 15$. The higher pressure coefficient and the lower maximum velocity obtained by the SKE and LRNKE models results in close agreement in the total pressure recovery coefficient, as shown in Fig. 7. The figure indicates also that the diffuser causes a decrease in the total pressure by about 35% due to viscous losses.
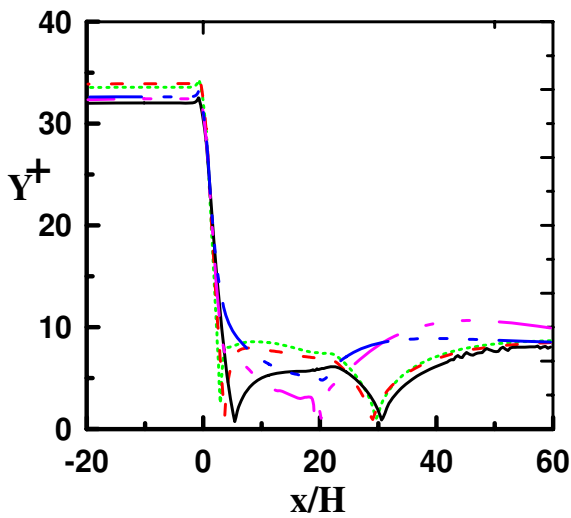
In order to provide a direct comparison with experimental data, results are presented by showing axial velocity, turbulent kinetic energy and Reynolds stresses profiles at several axial stations. Axial and vertical positions are non-dimensionalized

World Academy of Science, Engineering and Technology
International Journal of Aerospace and Mechanical Engineering
Vol:3, No:5, 2009

a- fine grid ($Y^+ \approx 1.0$) 421×79.

b- coarse grid ($Y^+ \approx 15$) 421×41

c- coarse grid ($Y^+ \approx 30$) 421×41

Fig. 4 Variations of Y^+ values for the tested turbulence models

by the upstream channel height, H, while the velocity profiles are normalized by the bulk velocity, U_b. The turbulent kinetic energy and Reynolds stresses are normalized by U_b^2. Fig. 8 shows a comparison between present predicted and measured velocity profiles at various axial locations along the diffuser for several turbulence models. The figure indicates that the SST, SKW and V2F models predict the axial velocity profiles very well, where. The RSM failed to predict the variation of axial velocity near the lower wall (i.e., in the separation zone). Similar observation was reported by Iaccarino [21]. This may be attributed to the use of the law of the wall for calculating the turbulence. On the other hand, the predicted axial velocity profiles using the LRNKE and the SKE models are in poor agreement compared with excremental data of [19]. This may be due to the inaccuracy of the isotropic turbulence models in predicting anisotropic turbulent flows, while the SST, SKW and V2F models contains some near-wall turbulence anisotropy.
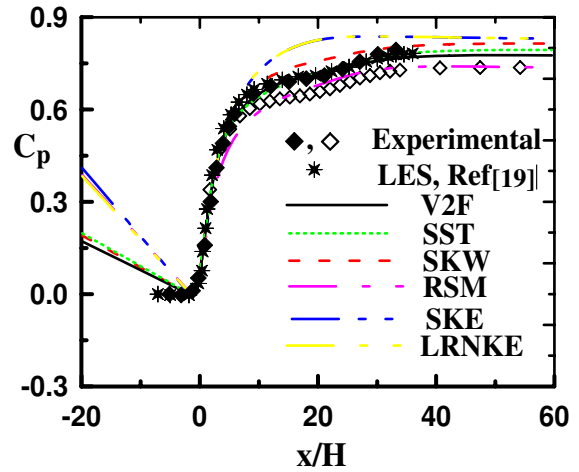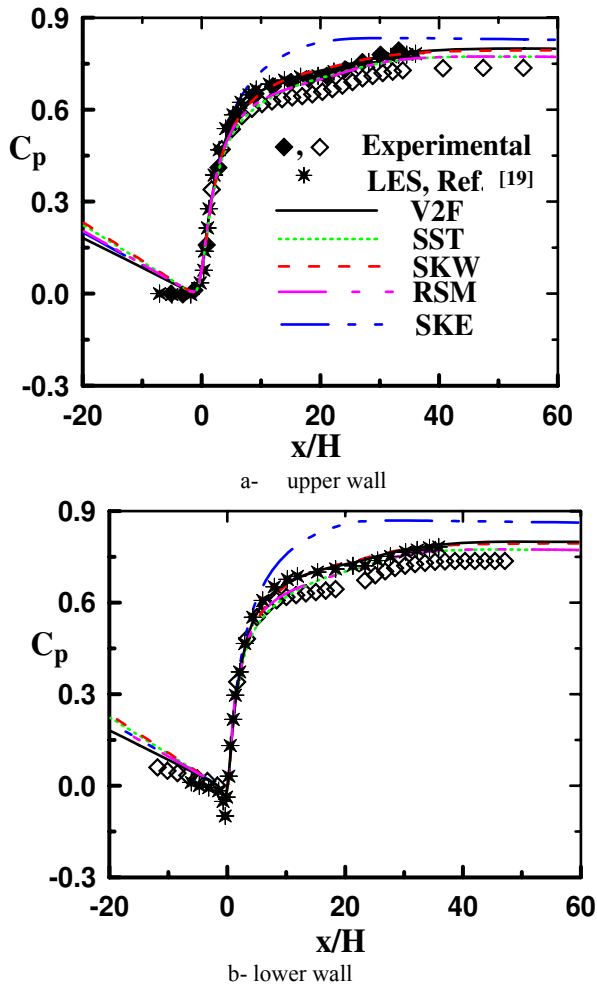

a- upper wall
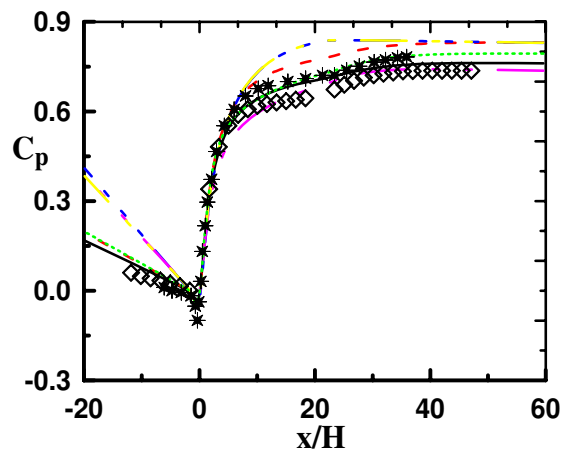
b- lower wall

Fig. 5 Comparison between present predictions, LES results of [19] and experimental results of [17, 18] in terms of pressure recovery, Cp for Y^+ =1.0 (closed symbols Obi et al. data [17], open symbols Buice-Eaton data [18])

World Academy of Science, Engineering and Technology
International Journal of Aerospace and Mechanical Engineering
Vol:3, No:5, 2009

a- upper wall

b- lower wall

Fig. 6 Comparison between present predictions, LES results of [19] and experimental results of [17, 18] in terms of pressure recovery, Cp for Y^+ =15 (closed symbols Obi et al. data [17], open symbols Buice-Eaton data [18])

The turbulent kinetic energy profiles are presented in Fig. 9. It can be seen from this figure that, at x/H = 5.2 all models except the V2F model over-predict the turbulent kinetic energy. Downstream at x/H = 11.2, 15.2, the SKW and V2F predictions are closed to each other and in a good agreement with the experimental data, while the SST and RSM over-predict the turbulent kinetic energy. Further downstream x/H=15.2, only the V2F model gives the best agreement between predicted and measured turbulent kinetic energy. It can be seen also from this figure that the LRNKE and SKE models completely fail to capture the asymmetric development of turbulent kinetic energy and underestimate its magnitude in the diffuser. The development of Reynolds stresses profiles is presented in Fig.10. Since the Reynolds stresses are available only for RSM in FLUENT, therefore, a user defined subroutine is written to calculate and store the Reynolds stresses for other models in three user defined memories, UDM. The figure shows that all models under-predict $\overline{u'u'}$ and over-predict $\overline{v'v'}$. Despite the SKW and V2F models

predict the turbulent kinetic energy better than the RSM, the latter predicts the Reynolds stresses better than other models. This can be attributed to the solution of separate transport equation for each component of the Reynolds stresses in the RSM model while they are calculated from the Boussinesq assumption in the other models.
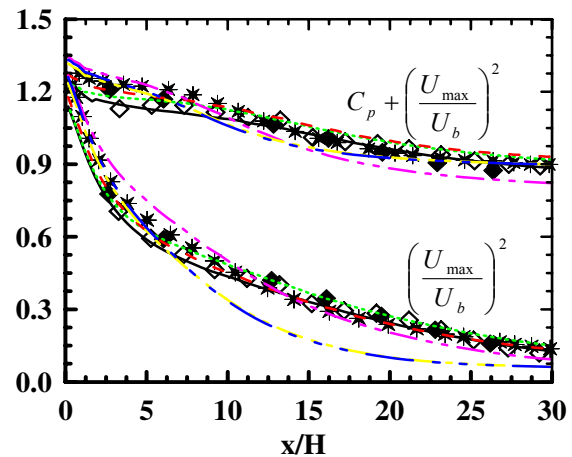

Fig. 7 Comparison of present predictions of pressure recovery C_p and U_{max}/U_b with experimental and LES results.
(Caption as in Fig. 6)

The skin friction coefficients on both the upper and lower wall for different turbulence models used in the case of fine and coarse grids are presented in Figs. 11-12. Firstly, from the figure it is seen that there is a notable difference between the prediction of friction coefficient using different turbulence models on both the upper and lower wall of the diffuser. The SKE and RSM models fail to predict the boundary layer separation and consequently the friction coefficient. This may be due to the use of the low of the wall in both simulations. However, the use of damping functions instead of the law of the wall in LRNKE model does not introduce any significant improvement. The V2F predicts a bubble in very close agreement with the experimental data of [18] and LES results of [19] at Y^+ = 1. The SKW and SST models predictions are in acceptable agreement. The figure also indicates that increasing the dimensionless wall distance, Y^+ to 15 enhances the predictions of the SKE and RSM models. However, further increase in Y^+ does not improve the predictions. The best prediction is obtained at Y^+ = 1 for the V2F model and at Y^+ = 15 for the SKW and SST models. At Y^+ = 15, the V2F under-predicts the skin friction coefficient in the upstream duct and along the upper wall of the diffuser. Fig. 13 shows a comparison between the present predicted skin friction coefficient along the upper and lower walls of the diffuser and that obtained by WIND code, Ref. [22]. The comparison shows a good agreement when SST model is used while the predictions from both codes are different when the SKE is used. The predictions obtained by the WIND code show a separation bubble at the upper of the diffuser wall which it was not observed experimentally. The very good agreement obtained when the SST model is used suggests that the

World Academy of Science, Engineering and Technology
International Journal of Aerospace and Mechanical Engineering
Vol:3, No:5, 2009

difference is not related to the numerical techniques used to discretize the equations but to the implementation of the SKE model. The evaluation of the wall normal distance, which is required in the law of the wall, may introduce such discrepancy.

The most common definition of the separation point is the location where the wall shear stress is zero. Table I shows a comparison between the experimental data of [18] and the present calculated separation point as well as the reattachment point using different turbulence models at different values of Y^+ and different grids based on C_f profiles. It can be seen from this figure that V2F model shows a good agreement compared with the other models. The SKW and SST models predicted the separation point earlier than that predicted by the V2F model and than the measured one. As Y^+ increases the RSM predicts a small separation region while the SKE and LRNKE models do not predict any separation. There are two other definitions found in the literature for the separation bubble. The first one is; the separation bubble is the mean

recirculating region within the dividing streamline (also called separation streamline) reaching between the stagnation points on the wall at the separation and reattachment points. The second definition is; the separation bubble is the region with mean backflow (i.e. region below the curve of zero mean velocity) [23]. Fig. 14 presents comparisons between the predicted position where the streamwise velocity crosses zero and the experimental data of [17 and 18] and LES results of [19], while the predicted dividing streamline is compared with LES results of [19] in Fig. 15. It can be seen from these figures that the separation bubble obtained from the experimental data is slightly larger than that obtained from the present predictions LES results. The present predictions using SKW and V2F models are in a close agreement with LES results when the finer grid is used, while a small discrepancy is introduced as Y^+ increase. The SST model gives the larger separation bubble compared with other models and LES results, while the RSM develops inaccurate results.
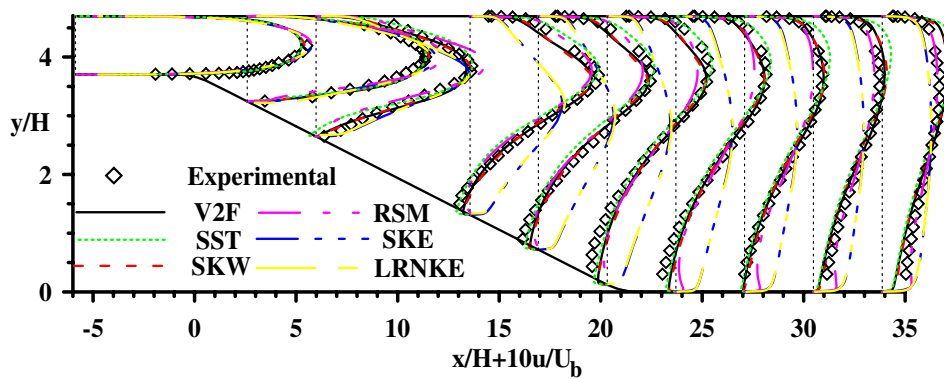

Fig. 8 Development of axial velocity profile through the diffuser for the tested turbulence models compared with and experimental results of Buice-Eaton data [18]
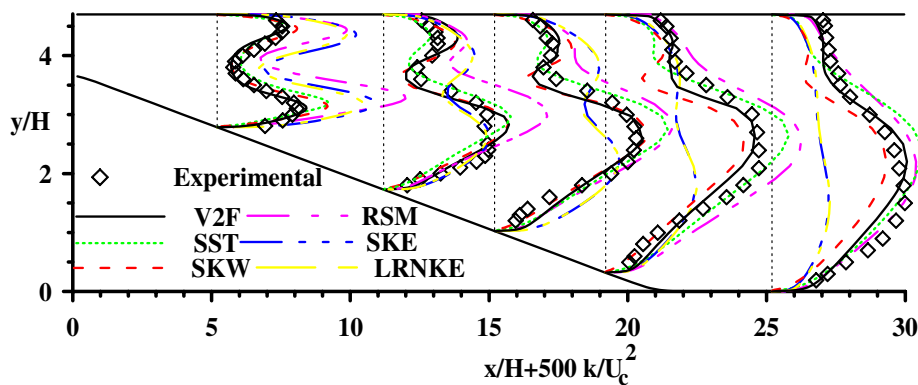

Fig. 9 Development of turbulent kinetic energy profiles through the diffuser for the tested turbulence models compared and experimental results of Obi et al. data [17]

World Academy of Science, Engineering and Technology
International Journal of Aerospace and Mechanical Engineering
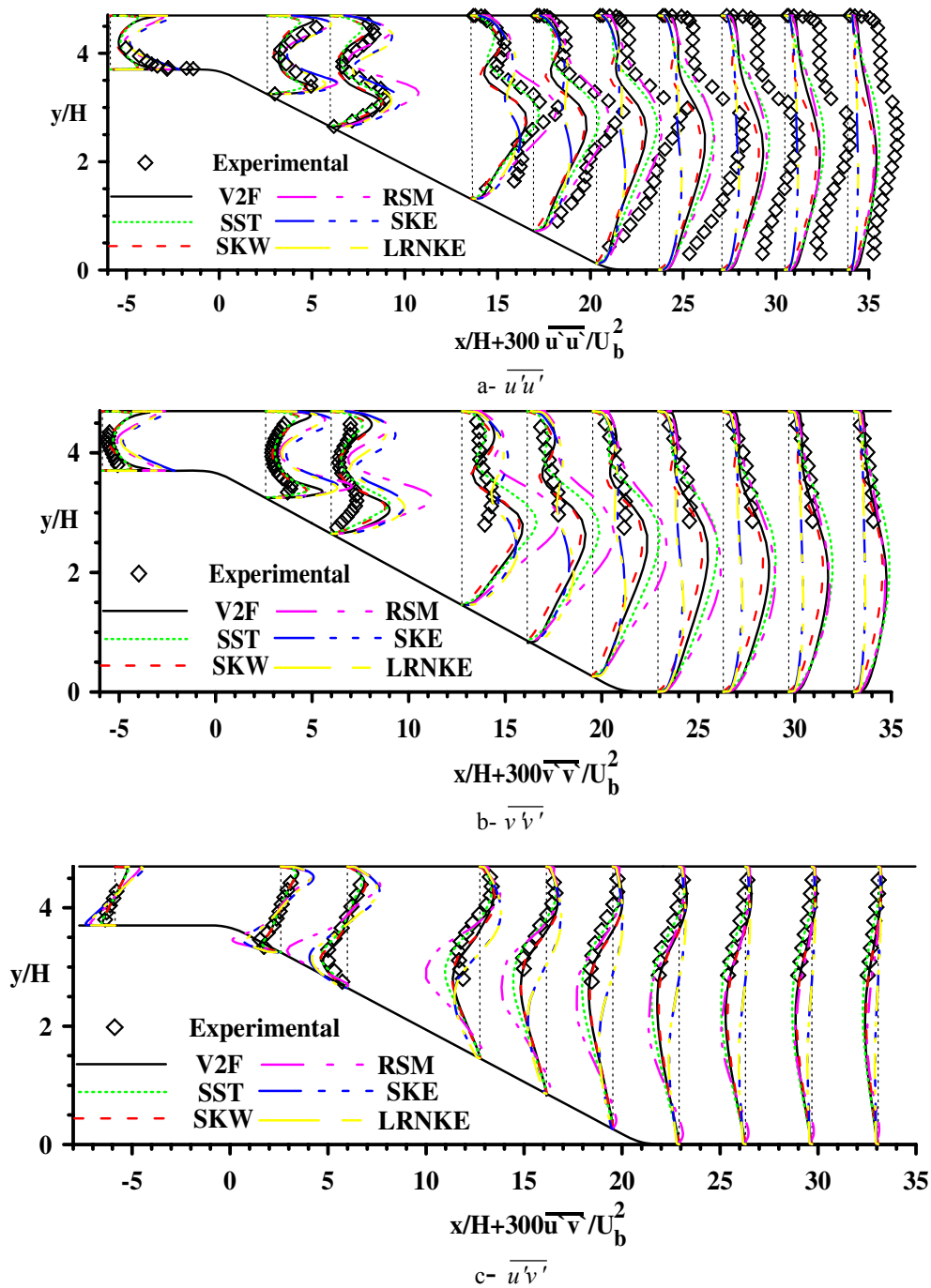Vol:3, No:5, 2009

Fig. 10 Development of Reynolds stresses profile through the diffuser for the tested turbulence models compared with experimental of Buice-Eaton data [18]

The computational effort and cost in terms of CPU time and number of iterations is shown in Table II. Generally, four factors influence the computing time namely, grid resolution, discretization scheme, degree of nonlinearity of the model, and number of PDEs the model contains. When fixing the first two factors, the difference in computing time is mainly attributed to the turbulence model itself. If the SKE model is taken as the baseline, then using the LRNKE and SKW models requires slightly more computation time and number

of iteration due to the extra terms and functions in the governing equations. Since the functions associated with the SST model are extra than that with SKW, it requires about 26 % grater time and about 13 % greater number of iteration than the SKE. Unlike the two-equation models, the V2F and RSM models require the largest time and number of iterations due to the extra transport equations (the number of differential equations to be solved is the same for two-dimensional problems). Despite of the comparable CPU time per iteration,

World Academy of Science, Engineering and Technology
International Journal of Aerospace and Mechanical Engineering
Vol:3, No:5, 2009

the RSM requires about 77% grater time than that of V2F due to the strong coupling between equations and the high degree of non linearity when the RSM is used.

a - upper wall

b - lower wall

Fig. 11 Comparison between present predictions, LES results [19] and experimental results of [17, 18] in terms of skin friction coefficient Cp for Y⁺ = 1.0 (closed symbols Obi et al. data [17], open symbols Buice-Eaton data [18])

IV. CONCLUSION

The turbulent flow through a planer asymmetric diffuser was investigated numerically using the commercial CFD code FLUENT 6.3.26. The performance of six different turbulence models is compared with published experimental and LES results. The standard k-ε, low-Re k-ε, standard k-ω, SST k-ω and RSM models are available as standard features in the code, while the v2-f model was implemented through the User Defined Functions in the code. The simulations was carried out on three grids having different spacing for the near wall points and different resolutions. The comparisons showed that V2F turbulence model indicates the best agreement with experimental data followed by the SKW and SST turbulence models. The SKE and LRNKE turbulence model give very poor results. Also, the RSM model gives unexpected poor

results compared with those obtained by V2F, SKW and SST model. In addition, the computational time and number of iterations required by each model are compared. The comparison showed that the RSM requires the greatest number of iterations and hence the largest computational time.
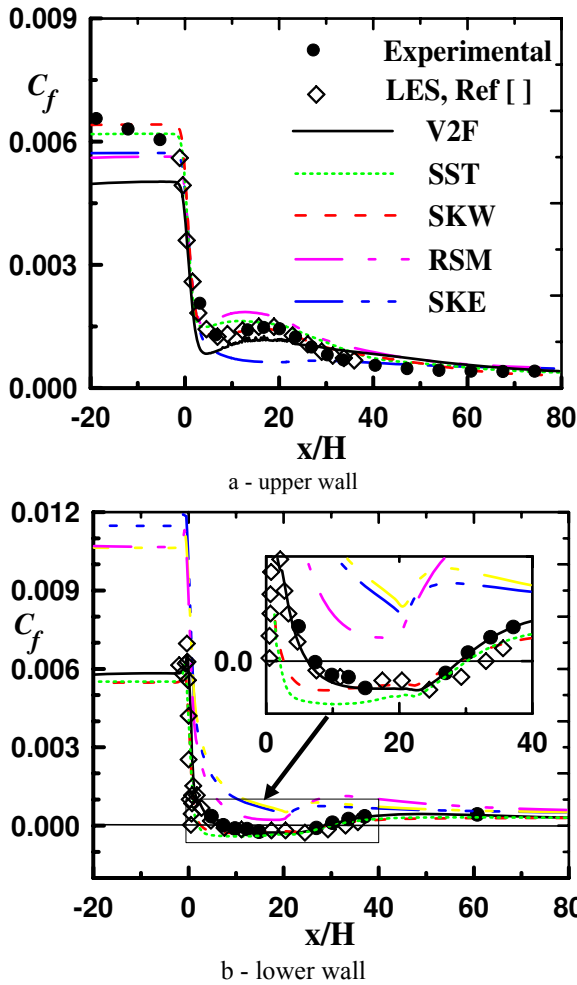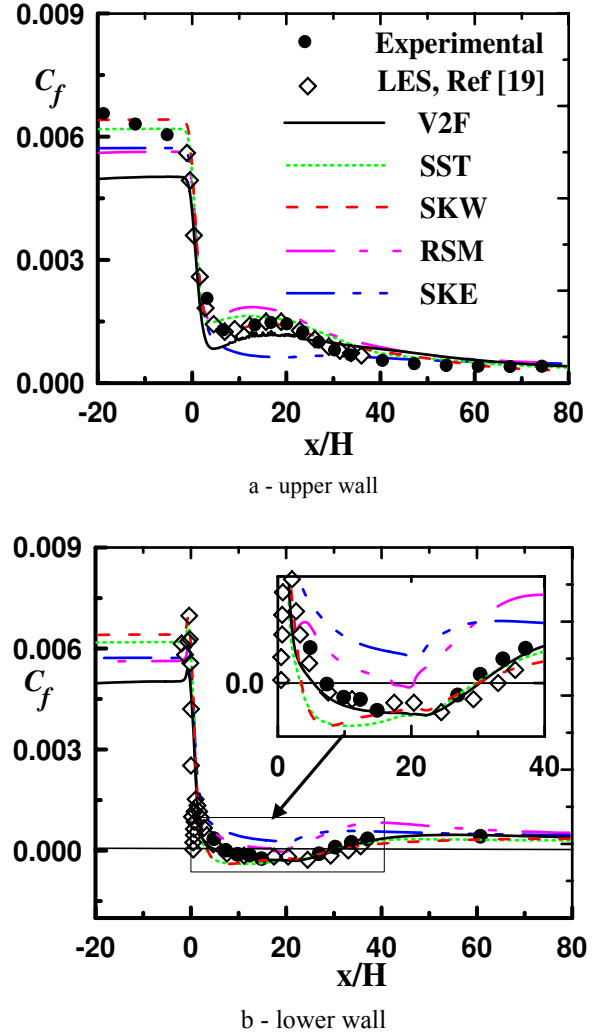

a - upper wall

b - lower wall

Fig. 12 Comparison between present predictions, LES results [19] and experimental results of [17, 18] in terms of skin friction coefficient Cp for Y⁺ = 15 (closed symbols Obi et al. data [17], open symbols Buice-Eaton data [18])

REFERENCES

[1] Wikipedia, "Computational fluid dynamics [online]", Available at http://en.wikipedia.org/wiki /Computational_ fluid_dynamics, [accessed Dec. 20, 2008].
[2] Bradshaw P., "Understanding and predictions of turbulent flow – 1996", Int. J. Heat and Fluid Flow, Vol. 18, 1997, pp. 45-54.
[3] Anderson D. A. and Tannehill, J. C. and Pletcher, R. H., "Computational Fluid Mechanics and Heat Transfer", Heimsphere Publishing Corporation, 1984.
[4] http://www.cfd-online.com/Wiki/ Turbulence _ modeling [accessed Dec. 20, 2008].
[5] Versteeg H. K. and Malalasekera W., "An introduction to computational fluid dynamics, the finite volume method", Longman group Ltd, 1998.

World Academy of Science, Engineering and Technology
International Journal of Aerospace and Mechanical Engineering
Vol:3, No:5, 2009

TABLE I
COMPARISONS BETWEEN PRESENT PREDICTED SEPARATION AND REATTACHMENT POINTS USING DIFFERENT MODELS AND EXPERIMENTAL DATA

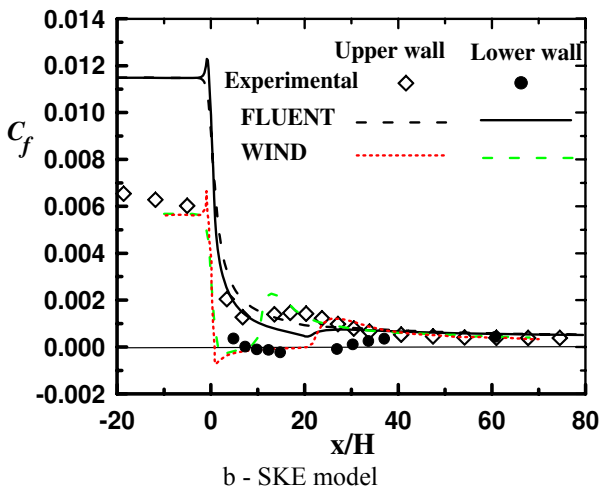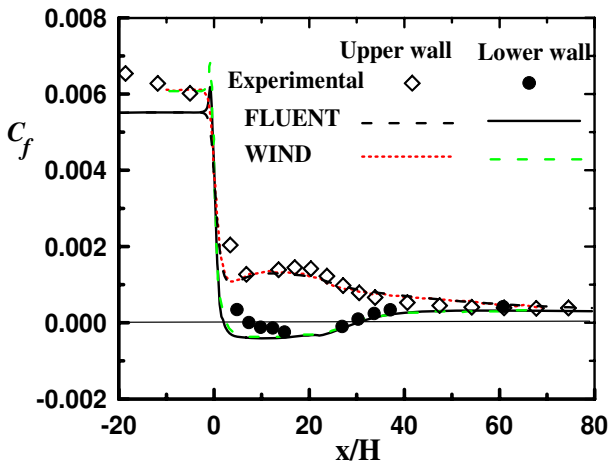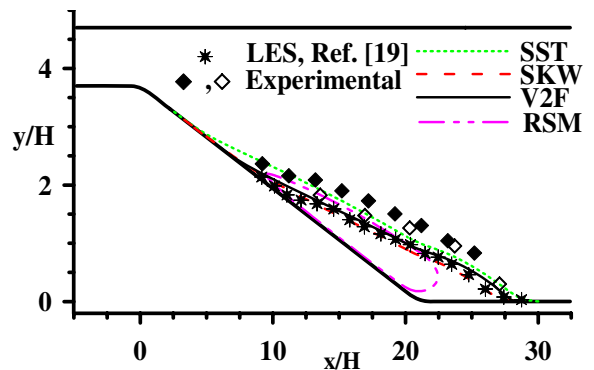| Grid		Exp.	SKW	SST	V2F	SKE	LRNKE	RSM
$Y^+ \approx 1.0$	Separation (x/H)	7.4	2.91	2.05	6.34	N/A	N/A	N/A
(421×79)	Reattachment (x/H)	29.2	28.95	30.15	29.25	N/A	N/A	N/A
$Y^+ \approx 15.0$	Separation (x/H)	7.4	3.51	3.38	5.32	N/A	−	17.04
(421×41)	Reattachment (x/H)	29.2	30.05	29.71	30.42	N/A	−	20.13
$Y^+ \approx 30.0$	Separation (x/H)	7.4	3.62	2.94	5.44	N/A	−	18.97
(421×41)	Reattachment (x/H)	29.2	28.92	29.53	30.72	N/A	−	20.25

a - SST Model

b - SKE model

Fig. 13 Comparison between present FLUENT predictions and predictions by WIND code, Ref. [22], using SST and SKE models and $Y^+ \approx 1.0$

[6] Launder B. E. and Spalding D. P., "The numerical computation of turbulent flows", Computer Methods in Applied Mechanics and Engineering, Vol. 3, 1974, pp. 269-289.

[7] Launder B. E. and Sharma B. I., "Application of the energy-dissipation model of turbulence to the calculation of flow near a spinning disc", Letters in Heat and Mass Transfer, Vol. 1, 1974, pp. 131-138.

[8] Yakhot, V. and Smith, L. M., "The Renormalization Group, the Epsilon-Expansion and Derivation of Turbulence Models", J. Scientific Computing, Vol. 7, 1992, pp. 35-51.

[9] Wilcox D. C., "Turbulence Modeling for CFD", DCW Industries, La Canada, California, 1998.

[10] Menter F. R., "Two-Equation Eddy-Viscosity Turbulence Models for Engineering Applications", AIAA Journal, Vol. 32, 1994, pp. 1598-1605.

[11] Durbin P. A., "Near-wall turbulence closure modeling without damping functions", Theoretical and Computational. Fluid Dynamics, Vol. 3, 1991, pp. 1-13.

[12] Launder B. E. and Spalding D. B., "Mathematical Models of Turbulence", Lectures Notes, Imperial College of Science and Technology, London, England, 1972.

[13] Patel V. C., Rodi W. and Scheuerer G., "Turbulence models for Near-wall and low Reynolds number flows: a review", AIAA J., Vol. 23, 1985, pp. 1308-1318.

[14] Fluent, "User's Guide Fluent 6.3.26", Fluent Incorporated, Lebanon, NH, 2006.

[15] Lien F-S and Kalitzin G, "Computations of transonic flow with the v2-f turbulence model", Int. J. Heat Fluid Flow, Vol. 22, 2001, pp. 5361.

[16] Kim J-Y, Ghajar A. J., Clementang and Foutch G. L., "Comparison of near-wall treatment methods for high Reynolds number backward-facing step flow", Int. J. Computational fluid dynamics, Vol. 19, 2005, pp. 493-500.

[17] Obi, S., Aoki, K., and Masuda, S., "Experimental and Computational Study of Turbulent Separating Flow in an Asymmetric Plane Diffuser," Ninth Symposium on Turbulent Shear Flows, Kyoto, Japan, August 16–19, pp. 305–1 to 305–4, 1993.

[18] Buice, C.U. & Eaton, J.K., "Experimental Investigation of Flow Through an Asymmetric Plane Diffuser," Journal of Fluids Engineering, vol. 122, pp. 433–435, 2000.

[19] Kaltenback H. J., Fatica M., Mittal R., Lund T. S., and Moin P., "Study of the Flow in a Planar Asymmetric Diffuser Using Large Eddy Simulations", J. Fluid Mech., Vol. 390, 1999, pp. 151–185.

[20] Patankar S. V., "Numerical heat transfer and fluid flow", McGraw-Hill, New York, USA, 1983.

[21] Iaccarino G., "Predictions of a turbulent separated flow using commercial CFD codes", Trans. ASME, J. Fluids Engineering, Vol. 123, 2001, pp. 819-828.

[22] DalBello T., "Computational study of separating flow in a planar subsonic diffuser", NASA TM 2005-213894, 2005.

[23] Törnblom O., "Experimental and computational studies of turbulent separating internal flows", Doctoral thesis, KTH Mechanics, Stockholm, Sweden, 2006.

a - $Y^+ = 1.0$

World Academy of Science, Engineering and Technology
International Journal of Aerospace and Mechanical Engineering
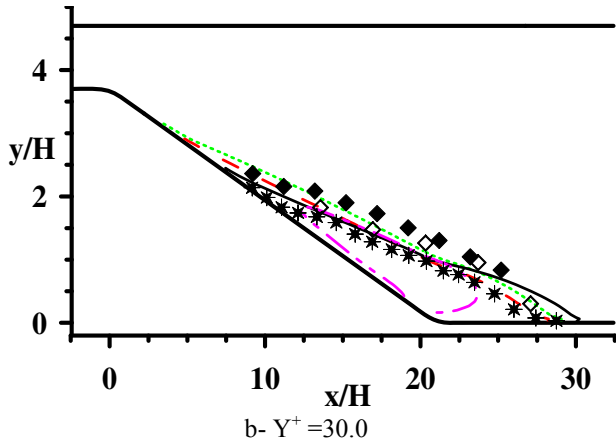Vol:3, No:5, 2009

b- Y^+ =30.0

Fig. 14 Position where streamwise velocity crosses zero compared
with LES results [19] and experimental results
of [17, 18] (closed symbols Obi et al. data [17],
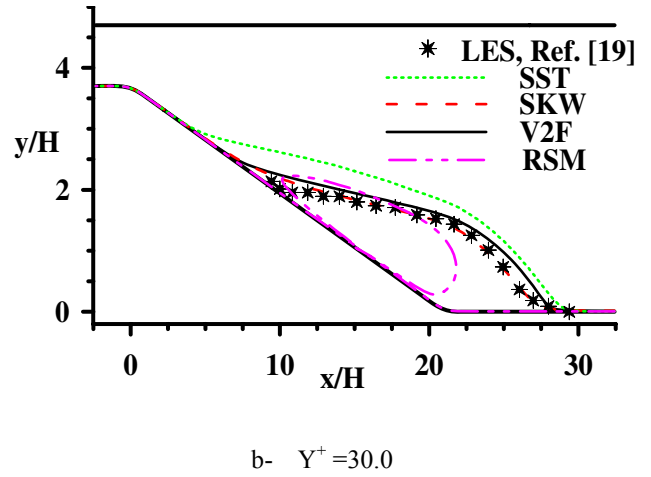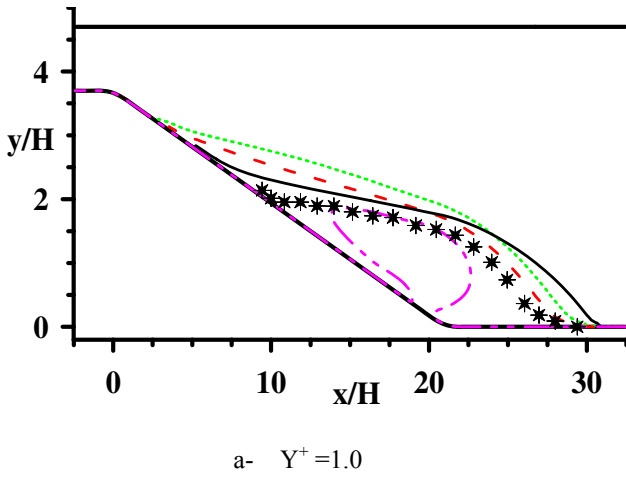open symbols Buice-Eaton data [18])

b- Y^+ =30.0

Fig. 15 Dividing (separating) streamline compared with LES
results [19].

a- Y^+ =1.0

TABLE II
NUMBER OF ITERATIONS AND CPU TIME NORMALIZED BY THOSE OF STANDARD k-ε MODEL

	SKE	LRNKE	SKW	SST	V2F	RSM
No. of iterations	1	1.03	1.07	1.26	1.2	2.06
CPU time	1	1.09	1.13	1.42	1.75	3.11
CPU time/iteration	1	1.06	1.06	1.13	1.46	1.51